iEMG: Imaging Electromyography

Holger Urbanek[a,*], Patrick van der Smagt[b,c]

[a] *Institute of Robotics and Mechatronics, Robotics and Mechatronics Center, German Aerospace Center (DLR), Oberpfaffenhofen, Germany*
[b] *Department of Informatics, Technische Universität München, Munich, Germany*
[c] *fortiss, TUM Associate Institute, Munich, Germany*

Abstract

Advanced data analysis and visualization methodologies have played an important role in making surface electromyography both a valuable diagnostic methodology of neuromuscular disorders and a robust brain-machine interface, usable as a simple interface for prosthesis control, arm movement analysis, stiffness control, gait analysis, etc. But for diagnostic purposes, as well as for interfaces where the activation of single muscles is of interest, surface EMG suffers from severe crosstalk between deep and superficial muscle activation, making the reliable detection of the source of the signal, as well as reliable quantification of deeper muscle activation, prohibitively difficult. To address these issues we present a novel approach for processing surface electromyographic data. Our approach enables the reconstruction of 3D muscular activity location, making the depth of muscular activity directly visible. This is even possible when deep muscles are overlaid with superficial muscles, such as seen in the human forearm. The method, which we call imaging EMG (*iEMG*), is based on using the crosstalk between a sufficiently large number of surface electromyographic electrodes to reconstruct the 3 D generating electrical potential distribution within a given area. Our results are validated by in vivo measurements of iEMG and ultrasound on the human forearm.

1. Introduction

The typical aim of recording surface EMG (sEMG) for kinesiology is to determine the relationship between movement and the activity of a certain set of muscles, through a model obtained by expert input, data input, or both. Expert input is usually based on physiological expertise, in which specific muscles are targeted as accurately as possible. Naturally, superficial muscles are usually targeted, as the activity of deeper muscles are seemingly obscured by superficial muscle activity.

*Corresponding author at: DLR German Aerospace Center, Robotics and Mechatronics Center, Institute of Robotics and Mechatronics, Münchner Straße 20, 82234 Weßling, Germany
Email address: holger.urbanek@dlr.de (Holger Urbanek)

Journal of Electromyography and Kinesiology 27, pp. 1–9, 2016
http://dx.doi.org/10.1016/j.jelekin.2016.01.001

In this paper we show that the latter is not necessarily true. By relating signal strength to muscle fiber distance over multiple sEMG electrodes, we can reconstruct volumetric muscular activity information in, e.g., the human arm. Based on the crosstalk between the electrodes, our method computes the position of the sources of the muscular activity measured on the skin. In the specific case we demonstrate, an array of 64 electrodes around the lower arm is used to determine the muscular activity within that arm. It renders a 3-D "picture" of the activity of the area covered by the electrodes. We refer to the method as Imaging EMG or *iEMG*.

The principle of reconstructing the sources leading to the EMG measurements is not new. Existing methods can be separated in *overdetermined* and *underdetermined* approaches. In the former case, single motor unit spikes are triangulated, where more electrodes are used than the number of simultaneous spikes to be detected. The methods work with the strong assumption that only a few single motor unit spikes occur simultaneously. In the latter, the distribution of the generating potential field is computed throughout a modeled volume.

Our proposed iEMG approach belongs to the class of underdetermined methods, as the number of possible distributions greatly exceeds the number of electrodes used. The solutions thus found may not be exact, but the method can be used to reconstruct muscular activity in any setting; even when multiple muscles at different depths are active.

Overdetermined methods.. If there are fewer motor unit spikes to be localized than there are electrodes, an exact solution can be found. The methods were pioneered by Gydikov et al. (1972) by localizing one single motor unit through sEMG. A simple volume conductor model was used to describe the propagation of the potential through the tissue:

$$P = a/d^n, \tag{1}$$

with P the amplitude of the potential at the electrode, d the distance between the electrode and the potential generated by the motor unit, and a and n constants. Kosarov et al. (1974) extended the method by automatically determining the damping constants a and n.

Monster & Chan (1980) calculated the origin of a single sEMG spike recorded using relatively few (from 3 to 9) surface electrodes by triangulating the peak-to-peak amplitude of a spike recorded from some electrodes, assuming that the potentials decay with a power function. Stonick et al. (1996) refined their earlier works (Jesinger & Stonick, 1994; LoPresti et al., 1995) to allow their algorithm to place multiple dipoles—up to approx. 10—within the volume of question.

The method described in (Roeleveld et al., 1997) uses the spread of the amplitude of a single motor unit activation over the skin surface. The authors verified their findings via intramuscular needle EMG, and could therefore show that their method works well as long as single activation potentials are detected.

Saitou et al. (1999) describe a method to estimate the number and location of motor units. This is done by distributing and simulating a small number of

motor units (from 1 up to 7) in a semi-infinite volume conductor. However, the results only allowed the estimation with relatively low muscle activations, since only then the activations on the motor units are discriminable. The detected depth of the motor units were <8 mm.

Underdetermined methods.. The second class of approaches tries to compute the distribution of the generating potential field within a volume. Even when the volume is discretized, the number of possible solutions exceeds the number of electrodes by far, barring analytical solutions.

Pioneering work has been published by van den Doel et al. (2008, 2011); here a method dubbed *computed myography* (CMG) is described for identifying the activation of individual muscles through the use of an sEMG array. Their method aligns arbitrary potentials to a fine grid and optimize while regularizing. The chosen regularizer introduces smoothness and penalizes potential spread.

Zhang et al. (2010) use a similar method—there called *muscle activity imaging* (MAI)—applied to simulated pelvic muscles, but a weighted minimum norm regularizer is used. They feed a mesh of the area in question into a FEM software as a forward model of the potential, where 22,174 dipoles are assumed to be evenly distributed in the model. The result is only simulated; no in vivo results are presented.

The same group presents with (Wang et al., 2012) another method for MAI that is based on Extended Kalman Filters together with a weighted minimum norm regularizer, which allows to incorporate temporal regularization in addition to the typical spacial one. In (Liu et al., 2014) this method is validated in vivo for single spikes with the ground truth stemming from a single needle electrode, gained from one single subject and one single position. The sEMG signal was gathered from 128 monopolar electrodes and it was beforehand decomposed for the single action potentials (AP). Since that method is used to localize single APs, it is some hybrid of the results gained by triangulation found in the overdetermined methods, and the mathematical approach of the underdetermined methods. So a regularizer is needed, and only a few APs can be detected at once.

Very recently Mesin (2015) presented a method for a rough but fast identification of active regions in muscles from sEMG measurements, focusing on a real-time applicability achieved by using pre-determined waveforms, and validated through simulations only.

Different from the minimum-norm regularizers that are used in the literature creating overly smooth solutions—(van den Doel et al., 2008, 2011; Mesin, 2015) use a Tikhinov Regularizer and (Zhang et al., 2010; Wang et al., 2012; Liu et al., 2014) a weighted minimum-norm regularizer—we present a regularizer which smooths only locally. Furthermore, we verify our approach *in vivo* by identifying the active muscles via ultrasonic imaging and comparing the resulting depths of activations of multiple subjects.

2. Methods

We call the source of the EMG potential (i.e., a muscle fiber) a *sender* and an sEMG electrode a *receiver*.

The activation of one receiver (i.e., one sEMG electrode), given the activation of all senders (namely the depolarized zone within a muscle cell), is based on the Cartesian distance of the electrode from the generating volume, as it can be derived from the volume conducting theory as presented in (Plonsey, 1977) or also in the simplified equation (1) with $n = 1$ as stated above for monopolar electrodes. However, the very exact relationship is not relevant for the theoretical considerations given, since it only influences the (arbitrary, but constant) term $d_{r,s}$ giving the influence of a sender s to the receiver r, summed as a linear combination of the activations, called *superposition principle*:

$$v_r = \sum_s v_s d_{r,s}, \tag{2}$$

with v_s as the activation of a sender s. So, all separate senders can be combined by simply summing their decayed values. Therefore, it is clear that also more sophisticated volume conductor models can be incorporated into $d_{r,s}$.

For notational simplicity we write $d_{r,s}$ as a matrix D, given that the number of receivers $|r|$ and the number of senders $|s|$ is finite:

$$\mathbf{v}_r = D\mathbf{v}_s. \tag{3}$$

This linear equation now needs to be solved with respect to $\mathbf{v}_s$, for which the Moore-Penrose pseudo inverse D^+ of D is useful:

$$\mathbf{v}_s = D^+\mathbf{v}_r. \tag{4}$$

This leads to a solution which is subject to a minimization with respect to the $\ell 2$-norm:

$$\arg\min_{\mathbf{v}_s} \|D\mathbf{v}_s - \mathbf{v}_r\|_2. \tag{5}$$

Because of the massively underdetermined nature of the problem, a direct solution without regularization is not viable.

Following what (Michel et al., 2004) described as "alternative source models," therefore following the reasoning of (Plonsey, 1982), the method proposed here does not try to place dipoles, which have a specific direction. Instead the secondary currents are assumed, generated by the action potentials within the volume conductor, which then are purely ohmic and therefore directionless current elements.

We regularize by putting neighboring senders into disjoint bins b. Each bin of senders can have an independent activation $v_{s,b}$. The number of bins, $|b|$, is set to be equal to the number of receivers $|r|$. The measured activation at

receiver r is defined as:

$$v_r = \sum_s v_s d_{r,s} \tag{6}$$

$$= \sum_b \sum_{s \in b} v_s d_{r,s}. \tag{7}$$

Since all v_s inside a bin b have the same activation, we call the activation inside a bin $v_{s,b}$. So we can continue:

$$v_r = \sum_b v_{s,b} \underbrace{\sum_{s \in b} d_{r,s}}_{:= d_{r,b}} \tag{8}$$

$$= \sum_b v_{s,b} d_{r,b} \tag{9}$$

$$\mathbf{v}_r = D_b \mathbf{v}_{s,b} \tag{10}$$

where D_b denotes the influence of a bin to each receiver. We can conveniently obtain the least-squares solution by solving

$$\arg\min_{\mathbf{v}_{s,b}} \|D_b \mathbf{v}_{s,b} - \mathbf{v}_r\|_2. \tag{11}$$

The binning results themselves deliver only a coarse representation of the real distribution of the electrical potentials. We solve this by repeatedly running the binning with random initial parameters, with additional arithmetic averaging over all solutions $\mathbf{v}_s$ gained through the random binning process. This results in a rather smooth activation distribution, where neighboring areas get similar activations.

It is can be shown that the mean of single valid solutions is again a valid solution of the original problem. Given different single n solutions $\mathbf{v}_{s_1}$ to $\mathbf{v}_{s_n}$,

$$\left.\begin{aligned} D\,\mathbf{v}_{s_1} &= \mathbf{v}_r \\ D\,\mathbf{v}_{s_2} &= \mathbf{v}_r \\ &\vdots \\ D\,\mathbf{v}_{s_n} &= \mathbf{v}_r \end{aligned}\right\} \quad \forall (i, k \in \{1, \ldots, n\} \mid \mathbf{v}_{s_i} \neq \mathbf{v}_{s_k}), \tag{12}$$

the mean of all solutions together,

$$D\left(\frac{\mathbf{v}_{s_1} + \cdots + \mathbf{v}_{s_n}}{n}\right) = \mathbf{v}_r, \tag{13}$$

is indeed a valid solution.

By averaging many of single solutions their common ground gets emphasized, resulting in a locally smooth solution. In contrast to other regularizers, the enforced smoothness is only local, where as on a global scope, the resulting

values may still diverge. The more electrodes are applied, the more local the smoothness gets, since the size of the bins decreases.

Since the potential fields are spatially determined, a binning process is preferred, which groups according to geometrical distance. With partitioning according to a Voronoi diagram with random seeds (called *Voronoi partitioning* herein) we found a suitable method for partitioning the volume based on geometrical distances.

The Voronoi diagram is defined as follows: Given a space X, a set of p seeds $s_p \in X$, and a distance metric δ , then for each s_k a region $R_k, k \in \{1, 2, \ldots, p\}$ can be defined as follows:

$$R_k = \{x \in X \mid \delta(x, s_i) < \delta(x, s_j)\ \forall i \neq j\}\,. \tag{14}$$

We take the distance metric to be Cartesian.

Another benefit of a geometrically-based binning is that prior model knowledge can be incorporated in the binning, e.g., the location of bones or precise muscular layout.

The method of binning by applying a Voronoi diagram will be called Voronoi Diagram Linear Randomized regularization (VDLR regularization).

3. Experiments

To show that the proposed iEMG method is working and does indeed lead to valid 3-D reconstructions of the muscular activity, it was applied to in-vivo sEMG measurements. To validate these first iEMG experiments, the measurements were compared to results measured with an ultrasound imaging system.

3.1. Setup

For the in-vivo measurements 64 sEMG electrodes are placed on the subject's forearm; distributed into four rings with 16 electrodes each.

The sEMG electrodes are sintered Ag/AgCl cup electrodes (Tallgren et al., 2005) by *GVB gelimed GmbH*, and have a total diameter of 10 mm while their conductive area has a diameter of 6 mm. An unshielded 1.5 m cable connects each electrode to the amplifier electronics. As conductive agent *Ten20 CONDUCTIVE* electrode paste by *Weaver and Company* is used. *Ten20* delivers nearly as good contacting properties as normal contact gels, but since it is pasty, it stays underneath each electrode and therefore prevents short circuiting between single electrodes. This is important for our setup in which electrode spacing is as small as 5 mm.

To assist in applying the electrodes, we constructed a holder with additional attachment points (see Figure 1). The holders are produced by a 3-D printing process using a non-conducting, mechanically strong and biologically harmless nylon (*polyamide 12*). Holes in the holders allow for application of the conductive gel. The attachment points allow for combining the electrode holders e.g. to a chain or to a ring. We chose an elastic chain *SUPER Elasto-Force* by

Figure 1: Cup electrode, electrode holder, and chained electrode holder.

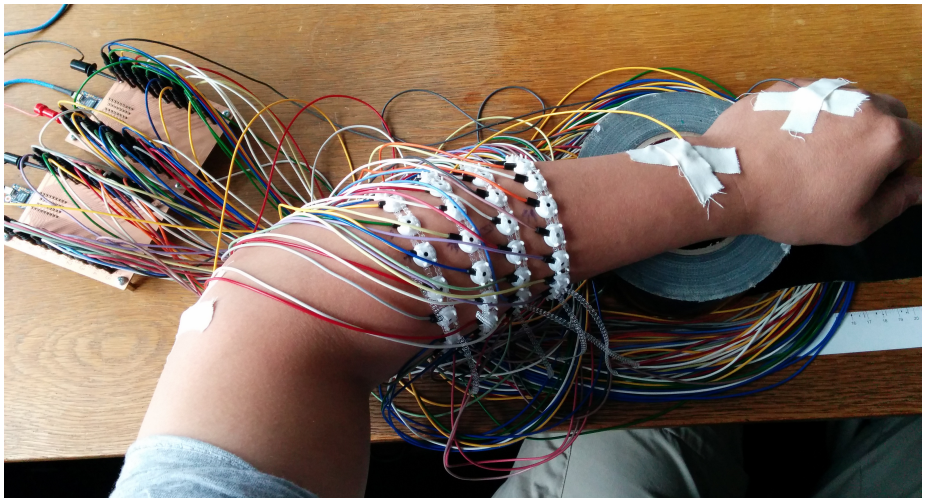

Figure 2: A forearm with 64 electrodes in 4 rings.

DENTAURUM[1], an intraoral elastic chain for dental use. The whole setup is shown in Fig. 2.

The electronics consists of the evaluation system *RHD2000* from *Intan Technologies* (Intan Technologies, 2014), where two 32-channel amplifiers *RHD2132* (Intan Technologies, 2013) are connected, allowing to measure up to 64 unipolar channels. We record all surface EMG data at 5 kHz.

The used amplifier and digitizer boards do a multiplexed sampling of 32 channels within 30 kHz each. If it is assumed that the fastest part of an action potential, the rising phase of the spike, has a duration of 1 ms, the error of the non-synchronous sampling is maximally $1/30 \approx 3.33\%$. Even though this effect is measurable, the effects on the reconstruction will be very little. So this effect is considered as being irrelevant for the given application.

3.2. Signal preprocessing

We place two interconnected reference electrodes, on the bony part of the elbow (*epicondylus lateralis*), the other on a bony part of the hand wrist (*processus styloideus ulnae*). The signals stemming from the electrodes are passed through three stages of preprocessing: (1) subtraction of the direct component, (2) rectification, and (3) integration over a fixed window. In the first step we reduce the influence of external signal noise by subtracting the average of all electrodes from each electrode. The preprocessed value of electrode m out of n at discrete time step t can then be written as

$$\tilde{r}_{m,t} = \sum_{i=t-l}^{t} |r_{m,i} - \overline{r}| \tag{15}$$

where $\overline{r} = \frac{1}{n}\sum_{i=1}^{n} r_i$ and l is the width of a time window over which is smoothed.

3.2.1. Additional assumptions

Within our proposed iEMG approach, we approximate the shape of the forearm by a cylinder. Simulations of the proposed method showed ample robustness against reasonable deformations of the arrangement of surface EMG electrodes. This has also been investigated for the particular case of elliptical deformations. Body fat is not specifically incorporated into the estimations of the recorded sEMG signals, since, different to traditional sEMG methods, iEMG will most likely place the sources of the potentials deeper into the tissue, ideally by the amount of the fatty tissue between the skin and the muscles. Of course, since fat has different electrical properties, more exact modeling, like the excellent model presented in (Blok et al., 2002), will allow for a better reconstruction at the cost of additional prior knowledge like the exact thickness of the fatty tissue.

Furthermore, we choose the number of partitions of Eq. (14) to be 1.5 times the number of electrodes. For the given 64 electrodes it is 96 regions. The

[1] REF 774-216-00.

slight increase of bins over the number of electrodes ensures mathematical stable solutions, since the conditioning of the linear equations improve. However, it is important that the number of bins still is "within sensible bounds", or else the inverse problem will collapse to the original state without any binning. The distribution of the Voronoi partitions is equal over the whole volume of reconstruction. No further anatomical knowledge, like the presence of bones or the different amount of muscle bellies, has been incorporated. The intention is to demonstrate the general applicability of the method. Naturally, more refined results are possible when the distribution of the partitions follows the anatomical structures, but we chose to demonstrate the methodology itself.

3.2.2. Verification via ultrasound imaging

We chose ultrasound imaging to acquire a ground truth to evaluate the results of the iEMG reconstruction. Our measurements were made with the *LOGIQ e*[2] manufactured by *GE Healthcare*. The ultrasonic probe is the GE *12L-RS*,[3], which is a wide-band linear array, allowing for a frequency bandwidth of 5–13 MHz. The probe is particularly suited for the signals we are interested in, viz. superficial muscles of the forearm[4]. The ultrasonic contact gel used is *echoson* by *SONOGEL Vertriebs GmbH*.

Since typical ultrasound imaging systems cannot image the whole forearm at once, they are not suitable to show that the whole reconstructed 3 D potential distribution is correct. However, ultrasound imaging can be used to check if the predicted depth of a potential's main source coincides with a major muscle activation. If a muscle contracts, it bulges, which can be seen in the ultrasound image.

Within this work a need for a maximal depth of about 4 cm was considered, so the ultrasonic device was tuned to use a frequency of 12 MHz, which allows to see about 3–4 cm deep with sufficient accuracy.

The 64 electrodes were placed at four rings of 16 electrodes each, at the upper part of the forearm. The rings were placed at about 6 cm, 8 cm, 10 cm and 12 cm distance from the elbow. Within each ring the electrodes were distributed in that way that the distance of each electrode to each neighbor within that ring was equal. We selected the placement of the four rings based on two criteria: first, there should be sufficient muscles to record underneath the chosen placement; and second, we need an arm diameter large enough to place 16 electrodes for a single ring.

After recording the surface EMG values, the position of each electrode was marked on the subjects forearms to assist the placement of the ultrasonic head. The subjects were instructed to reproduce the same "movement" during surface EMG and ultrasonic recordings. Compliance was visually inspected by the

[2]Model No.: 5148751.

[3]Model No.: 5141337.

[4]Specifications and intended purpose as described in the user manual of the *LOGIQ e* system and the manufacturers homepage at `http://www.gehealthcare.com/`.

experimenter.

To correlate the depths found by iEMG and ultrasound imaging, the same methods as described before were used. For iEMG, the depth according to a *center of area* (CoA), Δ_{CoA}, was calculated:

$$\Delta_{\mathrm{CoA}} := \frac{\sum_i \max({}^i v_s, 0)\Delta_i}{\sum_i \max({}^i v_s, 0)}, \tag{16}$$

with Δ_i the i-th depth value along a line, and ${}^i v_s$ the according linearly interpolated reconstructed iEMG value on that line with respect to Δ_i. For ultrasound, the means of the most shallow and the deepest value of the visually detected active muscles were calculated.

3.3. Experiments on 6 subjects

The experiments were conducted on 6 healthy male subjects, aged between 34–42 with mean at 37.

The muscle activation patterns were provoked by following movements: ring finger extension, middle finger extension, little finger extension, index finger extension, ring finger flexion, index finger flexion and little finger flexion. We constrained ourselves to single-finger movements to obtain dependable ground-truth data using ultrasound imaging, since in that case fewer muscles are involved. However, as shown in, e.g., Fig. 11, also more complex muscle activations can be reconstructed with our methodology. While restricting ourselves to single finger movements, we used all fingers which showed ample activation within the recorded area, which ruled out the thumb, but included ring and middle finger. The ring and middle finger are, of course, quite similar since the same muscles are involved for extension. Nonetheless this provoked some potential to verify the iEMG method against.

All those movements were produced against rigid structures with comfortably achievable maximal force,[5] so that no actual movement was produced, but the corresponding muscles are activated, to provoke an almost isometric contraction. The starting position was inspected by the experimenter to be similar between corresponding measurements (iEMG and ultrasound). Furthermore, the subject was instructed to pay attention to similarity.

For the given movements first the iEMG recordings were conducted, and when the iEMG showed significant activations without excessive recording artifacts, ultrasonic images were recorded and evaluated from a region with significant activation identified by iEMG. All measurements with ultrasonic recording are evaluated and included in the correlation presented later. This lead to 41 measurement pairs (iEMG and ultrasonic) distributed over the before mentioned 6 subjects.

Two pairs of recordings are exemplary detailed in the following, after which we will summarize the results.

[5] As it can be seen in equation (3) the strength of activation does not influence the volume conductor model D.

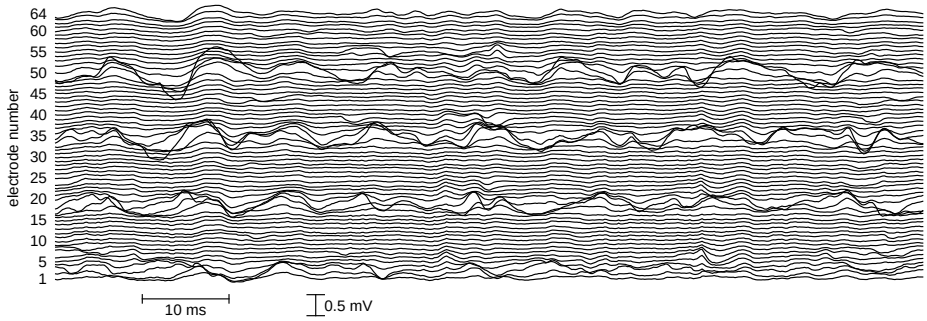

Figure 3: Raw electrode values for the extension of the left ring finger.

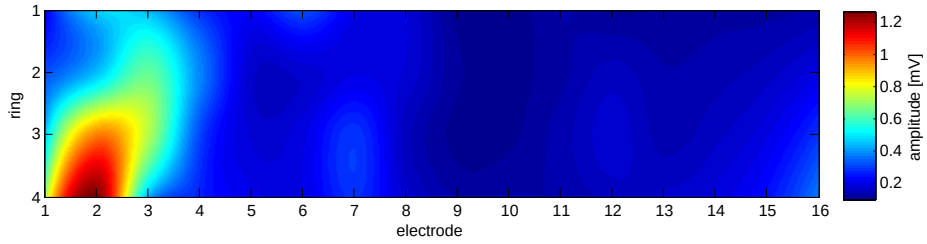

Figure 4: Interpolated amplitude map of the raw signal as in Figure 3 for the extension of the left ring finger.

Example: Ring finger extension. Figure 3 shows the raw surface EMG signals for each electrode, recorded at 5 kHz, which were used to generate the preprocessed electrode values depicted in Figure 5 by the use of equation (15) with a window width of 100 ms. In Figure 4 these raw EMG signals are presented as an interpolated amplitude map.

Figures 6 shows three cuts through the iEMG reconstructed 3 D volume of muscular activity. As a hint of the location for the cuts a schematic above each depicts the orientation of each cut: Left image—the ZY plane—is a horizontal cut through the arm, middle image—the ZX plane—a vertical cut and right image—the YX plane—is a cut perpendicular to the forearm. The approximate

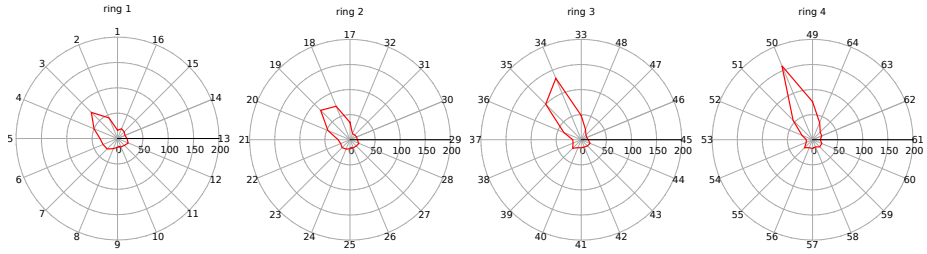

Figure 5: Rectified electrode values for the extension of the left ring finger.

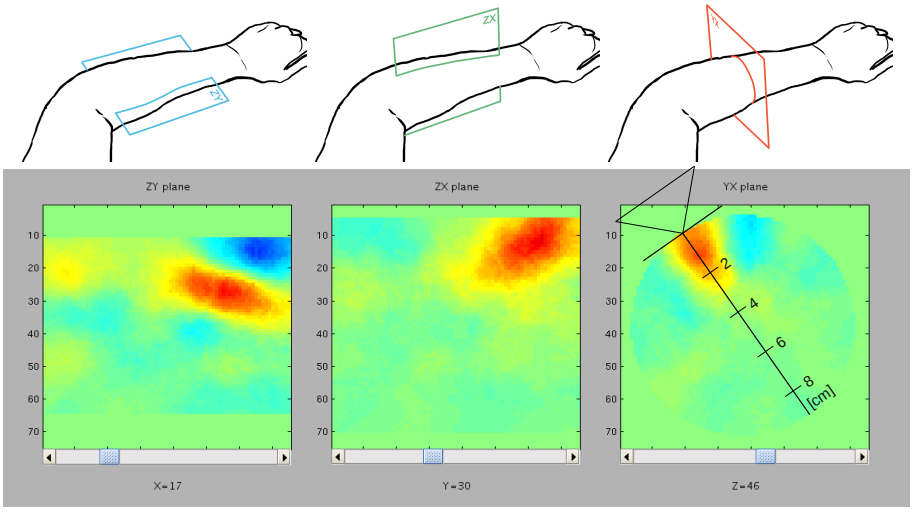

Figure 6: Left ring finger extension reconstructed with iEMG from the values shown in Figure 5.

placement of the ultrasonic probe is included in the cut through the YX plane, enhanced with an approximate scale for the depth. The iEMG reconstruction depicted here is based on 500 intermediate solutions, and the reconstructed area was inside a cube of $75 \times 75 \times 75$ voxels.

When extending the outstretched left ring finger against a rigid structure (so that almost no movement on the tendons is necessary) the iEMG image (Fig. 6) shows an increased activation in the outer area of the *Extensor digitorum* muscle as well as a muscle lying a bit deeper, possibly the *m extensor digiti minimi*. It could possible also be a deep *pollicis longus* muscle, but considering the instructed user movement this interpretation seems less likely. The reconstructed activation spreads from the surface to a depth of about 2–2.5 cm and a CoA value of 1.40 cm.

The preprocessed sEMG values of all 64 electrodes leading to that iEMG reconstruction are presented in Fig. 5. They are depicted as the 4 rings, ring 1 being proximal and ring 4 distal.

In Fig. 7 the right image is the ultrasound recording of the activated state, and shows bulging of two muscular structures, marked by arrows. This bulging is compared to the relaxed state imaged on the left. In the ultrasonic images a scale right of the images gives an approximation of the depth inside the tissue. Clearly a flatter structure right beneath the skin bulges (depth about .25–1 cm) and also a deeper structure shows bulging (depth about 1.25–2.5 cm). Visual inspection shows a good correspondence to the iEMG image.

Example: Index finger flexion. Figure 8 shows again the raw surface EMG signals for each electrode and in Figure 9 these raw EMG signals are presented as an interpolated amplitude map. The preprocessed EMG values are depicted

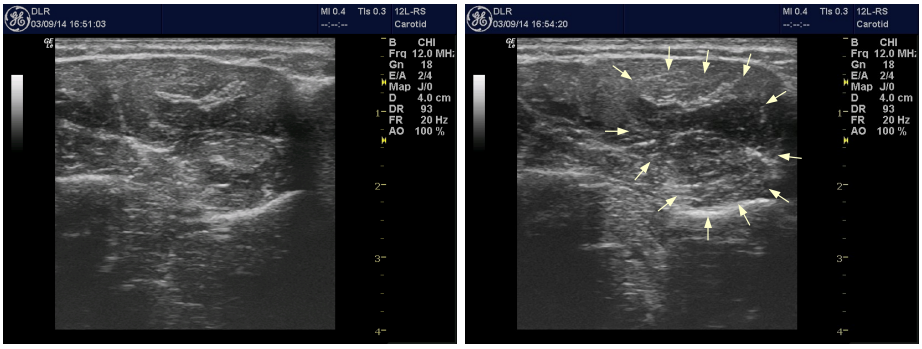

Figure 7: Left ring finger extension recorded with ultrasound, placed as depicted in Fig. 6; left image shows the relaxed state; the right image the activated state.

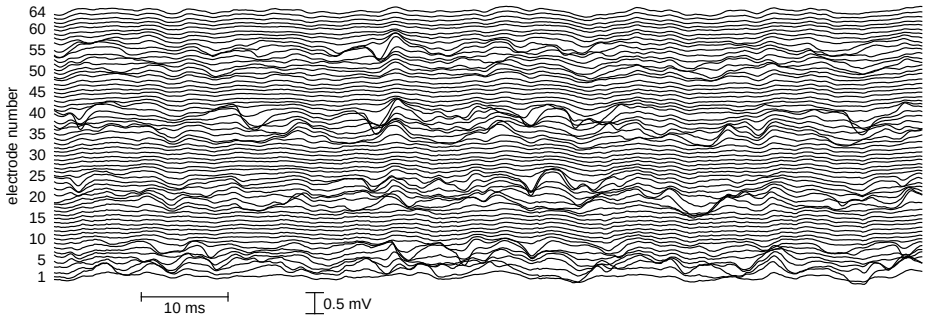

Figure 8: Raw electrode values for the flexion of the left index finger.

in Figure 10.

For the flexion of the outstretched left index finger against a rigid structure, the iEMG image (Figure 11) shows a major activation (depth 0–3.5 cm) for the *Flexor digitorum profundus* muscle and the *Flexor carpi ulnaris* and/or the *Flexor digitorum superficialis* muscle. The CoA of the iEMG reconstruction for that area computes to 1.78 cm.

With the ultrasonic image (Figure 12) it gets clearer that it is the *Flexor digitorum profundus* muscle (depth about 2.5–4 cm) and a small part of the *Flexor carpi ulnaris*, as marked in the ultrasonic image.

Here the iEMG image again compares well to the ultrasonic image. Just the small gap in activation between both muscles is not resolved by the iEMG image.

Correlation of experiments. When correlating all 41 measurements of the 6 subjects, a correlation factor of about 0.64 is gained. No outliers were removed to get this value. Figure 13 gives a visual representation of this relationship.

Here it can be seen, generally the depth as calculated from iEMG correlates well with the depth gained by ultrasonic imaging. For one subject, however,

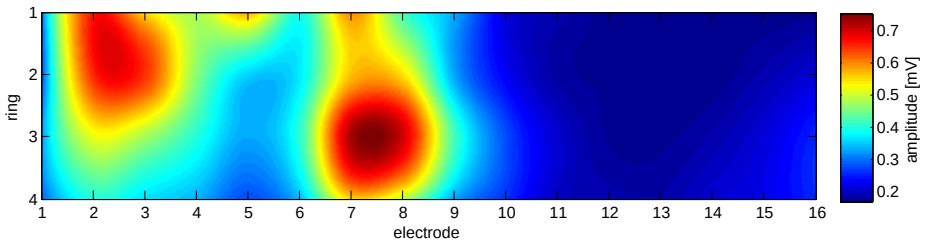

Figure 9: Raw electrode values for the flexion of the left index finger.

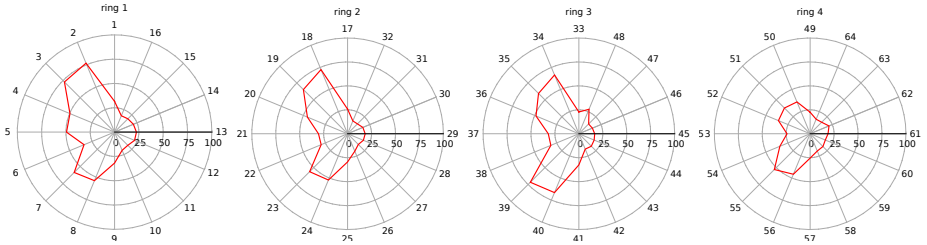

Figure 10: Rectified electrode values for the flexion of the left index finger.

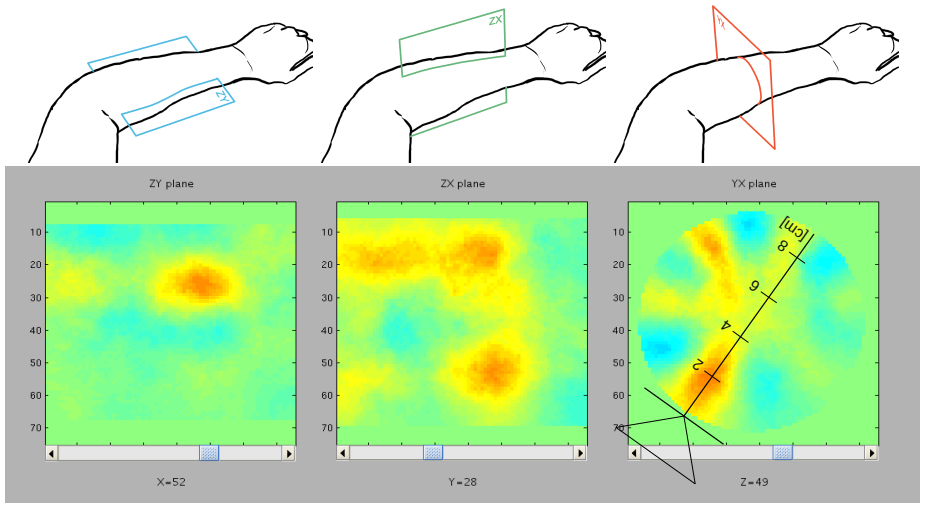

Figure 11: Left index finger flexion reconstructed with iEMG from the values shown in Figure 10.

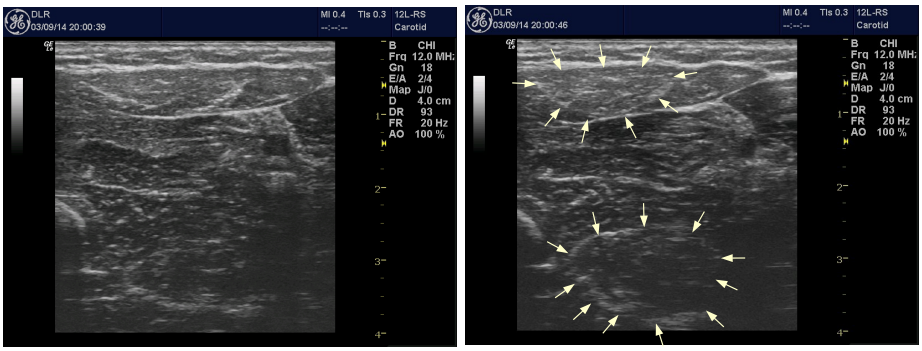

Figure 12: Left index finger flexion recorded with ultrasound, placed as depicted in Figure 11.

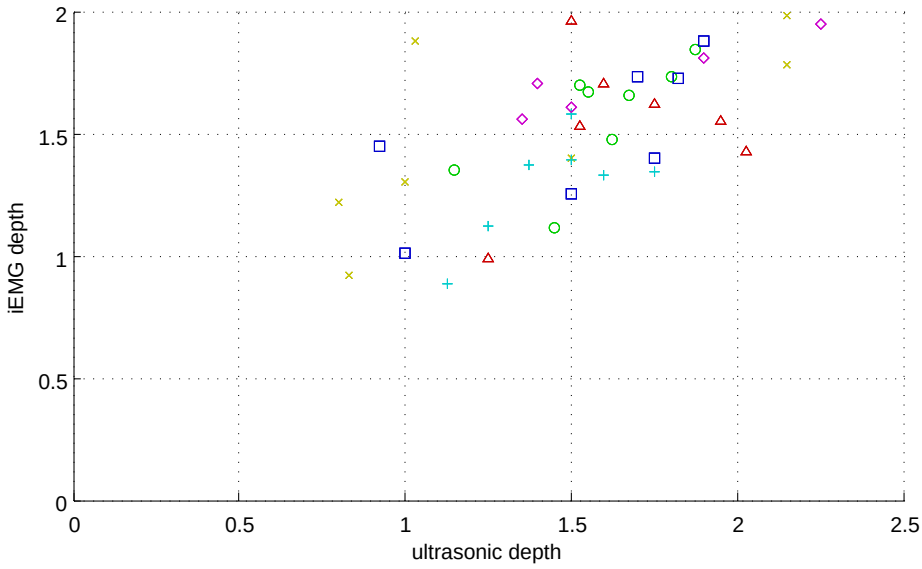

Figure 13: Correlation of the depth of muscular activity measured with iEMG versus ultrasonic imaging.

the correlation is not convincing: the subject depicted with a red triangle gives a correlation of only 0.24.

4. Discussion

We have demonstrated that our novel iEMG approach to reconstruct muscle activity—recorded from sEMG—in 3 D does work and exhibits ample robustness. Some open issues remain.

A more accurate ground truth for validating the iEMG is an important first step. However, intrafusal EMG does not provide a viable alternative, as the activation of single muscle fibers are not necessarily representative for whole muscle activation. MRI may give good results, see (Fleckenstein et al., 1992), but our measurement setup does not allow use in MRI environments.

Including detailed anatomical knowledge can enhance the iEMG algorithm to prevent activation in, e.g., bony or fatty areas. This can be achieved e.g. by excluding areas which cannot evoke potential from the partitioning process, and therefore no activations can be placed therein. Another possibility is to modify the Voronoi distance measure in such a way, that no partitions spread outside the region of a single muscle. But one major drawback of both suggested procedures is a typical one for detailed modeling: the errors from modeling, like the location of a bone is wrongly placed, the reconstruction may get even worse than with the more simple model. The same is true for a more sophisticated model of the volume conductor used in the model, like the one presented in (Blok et al., 2002). Nonetheless this needs to be investigated in detail for a further refinement of the presented method.

Within the optimization phase of the proposed algorithm even more norms should be researched and evaluated. It might prove that a specifically designed measure overcomes some of the problems of the presented method.

Aside this methodical issues, there are also some open questions regarding the technical implementation.

A huge speedup will be possible by executing large parts of the proposed algorithm on GPUs or computer clusters. The presented algorithm will scale well on both computing structures. On the one hand it is based on simple operations only (the complicated volume conducting model can be substituted by a look-up-table), which makes it especially suitable to be executed on graphics hardware. On the other hand, each intermediate solution is completely independent from the other intermediate results, so the calculation of those could be easily distributed to many computers. The application of these methods will bring the calculation time towards real time visualization capabilities.

Since the quality of iEMG imaging is hugely based on the number of electrodes, electrodes need to decrease in size. Also is it necessary to investigate the influence of electrode material and the feasibility to apply conducting supplements (without short circuiting between the electrodes). This topic is closely related to the improvement of fitting the electrodes. For more electrodes it also increases the demand for very high channel sEMG electronics, as well as the question to efficiently connecting them.

Blok, J. H., Stegeman, D. F., & van Oosterom, A. (2002). Three-layer volume conductor model and software package for applications in surface electromyography. *Ann Biomed Eng*, *30*, 566–577.

van den Doel, K., Ascher, U. M., & Pai, D. K. (2008). Computed myography: three-dimensional reconstruction of motor functions from surface EMG data. *Inverse Problems*, *24*, 065010. URL: http://stacks.iop.org/0266-5611/24/i=6/a=065010.

van den Doel, K., Ascher, U. M., & Pai, D. K. (2011). Source localization in electromyography using the inverse potential problem. *Inverse Problems*, *27*, 025008. URL: http://stacks.iop.org/0266-5611/27/i=2/a=025008.

Fleckenstein, J. L., Watumull, D., Bertocci, L. A., Parkey, R. W., & Peshock, R. M. (1992). Finger-specific flexor recruitment in humans: depiction by exercise-enhanced mri. *J Appl Physiol (1985)*, *72*, 1974–1977.

Gydikov, A., Kosarov, D., & Tankov, N. (1972). Studying the alpha motoneurone activity by investigating motor units of various sizes. *Electromyogr Clin Neurophysiol*, *12*, 99–117.

Intan Technologies (2013). *RHD2000 Series Digital Electrophysiology Interface Chips*. 11. December 2012; updated 5. September 2013.

Intan Technologies (2014). *RHD2000 Evaluation System*. 1. March 2013; updated 8. April 2014.

Jesinger, R. A., & Stonick, V. L. (1994). Processing signals from surface electrode arrays for noninvasive 3D mapping of muscle activity. In *Proc. Sixth IEEE Digital Signal Processing Workshop* (pp. 57–60). doi:10.1109/DSP.1994.379868.

Kosarov, D., Gydikov, A., & Tankov, N. (1974). Improvement of the method of motor units location. *Electromyogr Clin Neurophysiol*, *14*, 97–107.

Liu, Y., Ning, Y., He, J., Li, S., Zhou, P., & Zhang, Y. (2014). Internal muscle activity imaging from multi-channel surface emg recordings: a validation study. *Conf Proc IEEE Eng Med Biol Soc*, *2014*, 3559–3561. URL: http://dx.doi.org/10.1109/EMBC.2014.6944391. doi:10.1109/EMBC.2014.6944391.

LoPresti, E. F., Jesinger, R. A., & Stonick, V. L. (1995). Identifying significant frequencies in surface emg signals for localization of neuromuscular activity. In *Proc. IEEE 17th Annual Conf. Engineering in Medicine and Biology Society* (pp. 967–968). volume 2. doi:10.1109/IEMBS.1995.579384.

Mesin, L. (2015). Real time identification of active regions in muscles from high density surface electromyogram. *Comput Biol Med*, *56*, 37–50. URL: http://dx.doi.org/10.1016/j.compbiomed.2014.10.017. doi:10.1016/j.compbiomed.2014.10.017.

Michel, C. M., Murray, M. M., Lantz, G., Gonzalez, S., Spinelli, L., & de Peralta, R. G. (2004). EEG source imaging. *Clin Neurophysiol*, *115*, 2195–2222. URL: http://dx.doi.org/10.1016/j.clinph.2004.06.001. doi:10.1016/j.clinph.2004.06.001.

Monster, A. W., & Chan, H. (1980). Surface electromyogram potentials of motor units; relationship between potential size and unit location in a large human skeletal muscles. *Exp Neurol*, *67*, 280–297.

Plonsey, R. (1977). Action potential sources and their volume conductor fields. *Proceedings of the IEEE*, *65*, 601 – 611. doi:10.1109/PROC.1977.10539.

Plonsey, R. (1982). The nature of sources of bioelectric and biomagnetic fields. *Biophys J*, *39*, 309–312. URL: http://dx.doi.org/10.1016/S0006-3495(82)84521-9. doi:10.1016/S0006-3495(82)84521-9.

Roeleveld, K., Stegeman, D., Vingerhoets, H., & Oosterom, A. V. (1997). The motor unit potential distribution over the skin surface and its use in estimating the motor unit location. *Acta Physiologica Scandinavica*, *161*, 465–472. URL: http://dx.doi.org/10.1046/j.1365-201X.1997.00247.x. doi:10.1046/j.1365-201X.1997.00247.x.

Saitou, K., Masuda, T., & Okada, M. (1999). Depth and intensity of equivalent current dipoles estimated through an inverse analysis of surface electromyograms using the image method. *Med Biol Eng Comput*, *37*, 720–726.

Stonick, J. T., Jesinger, R. A., Stonick, V. L., & Baumann, S. B. (1996). Estimation and localization of multiple dipole sources for noninvasive mapping of muscle activity. In *Proc. Conf. IEEE Int Acoustics, Speech, and Signal Processing ICASSP-96* (pp. 2912–2915). volume 5. doi:10.1109/ICASSP.1996.550163.

Tallgren, P., Vanhatalo, S., Kaila, K., & Voipio, J. (2005). Evaluation of commercially available electrodes and gels for recording of slow EEG potentials. *Clin Neurophysiol*, *116*, 799–806. URL: http://dx.doi.org/10.1016/j.clinph.2004.10.001. doi:10.1016/j.clinph.2004.10.001.

Wang, J., Zhang, Y., Zhu, X., Zhou, P., Liu, C., & Rymer, W. Z. (2012). A novel spatiotemporal muscle activity imaging approach based on the extended kalman filter. *Conf Proc IEEE Eng Med Biol Soc*, *2012*, 6236–6238. URL: http://dx.doi.org/10.1109/EMBC.2012.6347419. doi:10.1109/EMBC.2012.6347419.

Zhang, Y., Wang, D., & Timm, G. W. (2010). A three-dimensional muscle activity imaging technique for assessing pelvic muscle function. *Inverse Problems*, *26*, 115018. URL: http://stacks.iop.org/0266-5611/26/i=11/a=115018.